Astronomy & Astrophysics manuscript no. accepted_v01
January 13, 2022
©ESO 2022

One size does not fit all: Evidence for a range of mixing efficiencies in stellar evolution calculations

C. Johnston[1,2]

[1] Department of Astrophysics, IMAPP, Radboud University Nijmegen, P. O. Box 9010, 6500 GL Nijmegen, the Netherlands, e-mail: cole.johnston@ru.nl
[2] Institute of Astronomy, KU Leuven, Celestijnenlaan 200D, 3001, Leuven, Belgium

Received 14 April 2021; accepted 13 July 2021

arXiv:2107.09075v2 [astro-ph.SR] 21 Jul 2021

ABSTRACT

Context. Internal chemical mixing in intermediate- and high-mass stars represents an immense uncertainty in stellar evolution models. In addition to extending the main-sequence lifetime, chemical mixing also appreciably increases the mass of the stellar core. Several studies have made attempts to calibrate the efficiency of different convective boundary mixing mechanisms, with sometimes seemingly conflicting results.
Aims. We aim to demonstrate that stellar models regularly under-predict the masses of convective stellar cores.
Methods. We gather convective core mass and fractional core hydrogen content inferences from numerous independent binary and asteroseismic studies, and compare them to stellar evolution models computed with the MESA stellar evolution code.
Results. We demonstrate that core mass inferences from the literature are ubiquitously more massive than predicted by stellar evolution models without or with little convective boundary mixing.
Conclusions. Independent of the form of internal mixing, stellar models require an efficient mixing mechanism that produces more massive cores throughout the main sequence to reproduce high-precision observations. This has implications for the post-main sequence evolution of all stars which have a well developed convective core on the main sequence.

Key words. Asteroseismology - Stars: interiors - Stars: evolution - Stars: oscillations (including pulsations) - Stars: binaries: eclipsing

1. Introduction

The treatment of convection and of convective boundary mixing has major implications for the results of stellar evolutionary models (Maeder 2009; Kippenhahn et al. 2012). As it is inherently a 3D process, the 1D descriptions of convection required for modern stellar structure and evolution calculations, often achieved using the Mixing Length Theory (MLT, Böhm-Vitense 1958) or variations thereof, have shortcomings. Although MLT does well in approximating the deep interiors of a convective region, its limitations become apparent at the boundaries of convective regions. Namely, MLT does not capture the scope of processes that occur over different distance scales at the interface of a turbulent convective zone and a stably stratified radiative zone. In such transition regions, phenomena including convective penetration, overshooting, turbulent entrainment, bulk shear mixing, and the generation of internal gravity waves which induce mixing in the adjacent radiative region may occur (Renzini 1987; Arnett et al. 2019). Additionally, 1D simplifications of convection result in a single, hard convective boundary (based either on the Schwarzschild or Ledoux criterion), rather than the dynamical, fluctuating boundary that is often observed in 2- and 3D hydrodynamical simulations (Meakin & Arnett 2007; Arnett et al. 2015; Cristini et al. 2017; Higl et al. 2021). As a result of ignoring the non-local extensions of convection, simplified 1D descriptions of convection underestimate the transport of chemical species both at the convective boundary and throughout the adjacent radiative region. More specifically, in the absence of some form of explicitly included extra chemical mixing, 1D stellar models with a convective nuclear burning core underestimate the transport of fresh chemical species from the envelope into the core where they can participate in burning. This implies that models which do not include extra mixing underestimate the mass of the convective core at any time along a star's evolution when the core is convective (Bressan et al. 1981; Stothers & Chin 1981; Bertelli et al. 1985; Maeder & Meynet 1987).

To account for the missing chemical mixing induced at convective boundaries, 1D stellar evolution models introduce ad-hoc parameterised mixing profiles that are stitched to convective regions. However, each parameterised mechanism only serves to address one aspect of the many processes occurring at, or beyond, a convective boundary (Meakin & Arnett 2007; Arnett et al. 2015; Rogers & McElwaine 2017). Furthermore, all of these parameterised descriptions have at least one free parameter that scales the 'efficiency' of the chemical mixing induced by that mechanism. Numerous studies have attempted to observationally calibrate the efficiency of different mixing mechanisms both at the convective boundary and in the radiative envelope, however, these studies often report conflicting efficiencies for the same mechanisms. The focus of this paper is to discuss the complexities of observationally constraining the efficiency of mixing mechanisms in stellar models, to introduce convective core mass as a robust point of comparison for the implementation of chemical mixing in 1D stellar models, and to consider the consequences of a range of inferred mixing efficiencies in model calculations.

2. Chemical mixing in the literature

A complete chemical mixing profile should include the effects of entrainment, penetration, overshooting, semi-convection, as well as mixing induced by rotational instabilities and internal gravity waves (Langer 2012; Maeder 2009; Hirschi et al. 2014; Arnett et al. 2015; Rogers & McElwaine 2017; Salaris & Cassisi 2017). Unfortunately, discussion of chemical mixing mechanisms in the literature suffers from a problem of mixed identities. Numerous studies have attempted to constrain the impact of chemical mixing in different forms, be it any of the mechanisms previously mentioned. However, more often than not, these studies focus on constraining the efficiency of a single mixing mechanism, fixing the efficiency of the other mechanisms or ignoring them outright. In the process of doing this, one effectively enforces that the mixing mechanism under investigation in practice becomes a proxy for all of the chemical transport present. Thus, when comparing results of different studies, one must account for both the physical mechanisms that were explicitly included, as well as the absence of effects from any physical mechanisms that were not included.

Given modern observational quantities, their associated precision, and underlying model assumptions and degeneracies, we are unable to disentangle the contributions of individual mixing mechanisms to the point of robustly calibrating multiple mixing mechanisms in a single target (Valle et al. 2017, 2018; Constantino & Baraffe 2018; Aerts et al. 2018; Johnston et al. 2019c). Instead, different observables provide constraints on the overall mixing history of a star. We will briefly review the types of observations used to constrain chemical mixing in the literature.

2.1. Eclipsing Binaries

If the two components of a double-lined spectroscopic binary system eclipse, one can model the eclipses and radial velocities to determine absolute masses and radii of the components. Combined with effective temperature estimates from spectroscopy, modelling eclipsing binaries provides some of the most precise determination of fundamental stellar properties possible, with quoted uncertainties to better than one percent on mass and radius (Torres et al. 2010; Serenelli et al. 2021). Furthermore, binaries afford the assumption that both components have the same age and initial chemical composition, providing additional powerful constraints.

The standard approach in the literature is to fit stellar evolution models (or isochrones) to the observed mass, radius, and temperature of the binary components to determine how much internal mixing, if any, is required to explain observations of intermediate- to high-mass stars with a convective core on the main sequence. This approach has been used to investigate the impact of rotational mixing (Brott et al. 2011b; Schneider et al. 2014b; Ekström et al. 2018), convective penetration (Schroder et al. 1997; Pols et al. 1997; Ribas et al. 2000; Guinan et al. 2000; Claret & Torres 2016), and convective overshooting (Stancliffe et al. 2015; Higl & Weiss 2017; Claret & Torres 2019; Costa et al. 2019; Tkachenko et al. 2020). However, notable works claim that chemical mixing efficiency cannot be uniquely determined using this approach, even with such precise mass and radius estimates (Valle et al. 2018; Constantino & Baraffe 2018; Johnston et al. 2019b). Similarly, systems that display apsidal motion have been used to investigate chemical mixing through its influence on the central condensation of the star over time (Claret & Giménez 2010; Claret 2019).

We note, however, that the fundamental stellar properties used in this modelling method are not directly sensitive to the efficiency of any particular mixing mechanism individually. Instead this methodology is sensitive to the efficiency of any process which alters the radius and temperature of the star. Through the transport of hydrogen from the envelope into the core, chemical mixing increases the mass (and luminosity) of the core, and extends the main-sequence lifetime. These changes to the core translate to changes in the overall temperature and radius of the star at a given age, which is what is estimated in binary modelling. Furthermore, in addition to the transport of chemicals in the interior, very rapid rotation causes changes to the radius and temperature at the surface of the star. Thus, modelling the fundamental properties of binaries is sensitive to the total internal mixing history which transports fresh hydrogen from the radiative region into the convective core throughout the stellar lifetime, as well as any modification to the surface properties due to rapid rotation. To this end, we should be careful to not conflate the inferred overall mixing efficiency from binary modelling with the efficiency of a single mixing mechanism.

2.2. Stellar clusters

Given the assumption that the members of a stellar cluster are formed at approximately the same time and with a similar initial chemical composition, the observed morphology of the colour-magnitude diagram can be used to calibrate internal mixing mechanisms in stellar models. Several studies have demonstrated that the width of the main sequence is sensitive to the mixing history of stars, and used this sensitivity to estimate the effect of overshooting and/or rotational mixing on stellar models (VandenBerg et al. 2006; Castro et al. 2014; Martinet et al. 2021).

Similar to the width of the main sequence, the morphology of the extended main-sequence turn off (eMSTO) is used to test the implementation of mixing mechanisms in stellar models. While the eMSTO phenomenon is commonly associated with rapid rotation and its consequences (Dupree et al. 2017; Kamann et al. 2018; Bastian et al. 2018; Georgy et al. 2019), studies have shown that the eMSTO of young massive clusters can be reproduced by stellar evolution models with convective boundary mixing calibrated from asteroseismology (Yang & Tian 2017; Johnston et al. 2019a). Alternatively, binary evolution and its byproducts have been invoked as a means of explaining the eMSTO phenomenon (Schneider et al. 2014a; Gosnell et al. 2015; Beasor et al. 2019). As in the case of eclipsing binaries, this type of analysis is not directly sensitive to the efficiency of a given mixing mechanism, but rather to the total mixing across the evolution of a star.

2.3. Asteroseismology

Regions of the stellar interior can be driven to deviate from hydrostatic equilibrium due to a build up of radiation caused by partial ionisation zones, the blocking of convective flux, or other mechanisms. Depending on where these perturbations occur within the stellar interior, the restoring force will be dominated by either the pressure force or the buoyancy force. If a perturbation is regularly driven, it produces a standing pressure or buoyancy wave propagating throughout the star, resulting in surface brightness and velocity variations. The frequency of the standing wave is determined by the chemical and thermodynamical conditions of the regions that the waves travel through. As-

teroseismology is then the study of the stellar interior via the observation of and modelling of stellar oscillations (Aerts et al. 2010; Aerts 2021).

The frequencies of g modes (buoyancy waves) in particular are sensitive to the near-core chemical gradient (Miglio et al. 2008) and rotation rate (Bouabid et al. 2013). Asteroesismology of stars oscillating in p modes and in g modes with $1.3 \leq M \leq 24$ $M_\odot$ has revealed the need for a wide range of convective boundary mixing efficiencies to reproduce observed pulsation frequencies (Briquet et al. 2007; Handler 2013; Moravveji et al. 2016; Schmid & Aerts 2016; Szewczuk & Daszyńska-Daszkiewicz 2018; Mombarg et al. 2019; Pedersen et al. 2021). Additionally, asteroseismology of stars pulsating in p modes (pressure waves) between 1.15-1.5 $M_\odot$ has revealed the need for a range of convective mixing efficiencies to reproduce observed frequencies (Deheuvels et al. 2010; Deheuvels & Michel 2011; Silva Aguirre et al. 2011; Salmon et al. 2012; Angelou et al. 2020; Viani & Basu 2020; Noll et al. 2021). Similar to binaries and clusters, the modelling of pulsation frequencies (for both p and g modes) is not sensitive to the efficiency of a single mixing mechanism. Instead asteroseismology is sensitive to the total influence of chemical mixing that alters the core mass and radius, as well as the chemical gradient near the core (high order g modes) and the bulk density of the star (low order p and g modes). However, studies have demonstrated that g-mode asteroseismology is able to differentiate between the morphology and temperature gradient of the near core mixing profile for models of the same mass evolved to the same core hydrogen content (Pedersen et al. 2018; Michielsen et al. 2019).

3. Convective core masses

Despite the remarkable precision provided by eclipse modelling and/or asteroseismology, modelling methodologies cannot uniquely constrain the efficiency of an individual mixing mechanism (Valle et al. 2018; Aerts et al. 2018). Unfortunately, parameter correlations in stellar evolution models can produce several models with different masses, ages, and amounts of internal mixing that all reproduce observations reasonably well within the uncertainties. As such, it is often the case that any amount of internal mixing can be used to match observations, even when the bulk stellar properties or oscillation frequencies are known to a high precision (e.g., Aerts et al. 2018; Constantino & Baraffe 2018; Johnston et al. 2019c,b; Michielsen et al. 2019; Sekaran et al. 2021). Furthermore, both binary and asteroseismic studies have demonstrated that reasonably similar fits to the data can be obtained using models with different types of internal mixing mechanisms (Moravveji et al. 2015; Claret & Torres 2017; Mombarg et al. 2019; Pedersen et al. 2021) and for different bulk chemical compositions (Claret & Torres 2017, 2018).

Although model degeneracies prevent the direct constraining of mixing mechanism efficiencies, Johnston et al. (2019b); Tkachenko et al. (2020) demonstrated that 1% precision on mass and radius estimates from eclipsing binaries result in inferences on the mass and hydrogen content of the convective core to a precision of $\sim$ 10 % or better. A similar result has been found through asteroseismic analysis of both p and g mode pulsating stars with a convective core on the main sequence (Mazumdar et al. 2006; Briquet et al. 2011; Johnston et al. 2019c; Angelou et al. 2020; Mombarg et al. 2021; Pedersen et al. 2021).

A few studies have performed comparative model fits between models with an exponentially decaying diffusive overshooting with a radiative temperature gradient in the overshooting region and models with step penetrative convection with

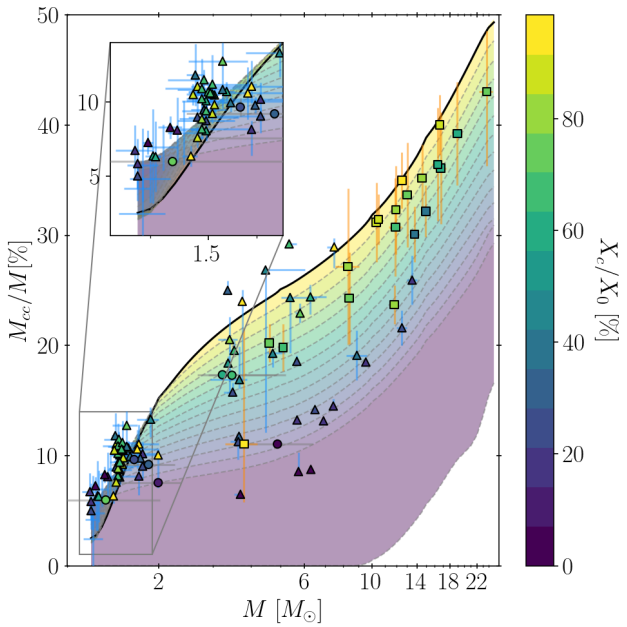


Fig. 1. Convective core mass (M_{cc}) vs initial mass (M) of the star. Solid and dashed lines correspond to fractional core mass at specified points in evolution. Colour of region corresponds to fractional core hydrogen content as indicated by colour-bar. Colour of individual marker corresponds to inferred fractional core hydrogen content of best model. Squares with orange uncertainties denote values obtained from binary systems, circles with blue uncertainties denote values obtained from binary systems with at least one pulsating component, and triangles with grey uncertainties denote values obtained from pulsating stars. References for values and their uncertainties are listed in Table A.1.

an adiabatic expansion of the convective core. These studies demonstrate that the best matching solutions from either model have core masses, masses, and ages, which largely agree within uncertainties (Claret & Torres 2018; Tkachenko et al. 2020; Mombarg et al. 2021; Pedersen et al. 2021). However, it should be noted that solutions with different metallicities tend to have different core mass inferences, masses, and ages as well. This highlights that core mass inferences can function as a robust proxy for the overall influence of chemical mixing, even when the efficiency of the implemented mechanism cannot be constrained. Furthermore, this implies that core mass inferences can serve as a robust comparison point for solutions that do not use the same implementation of chemical mixing.

To this end, we collect a large sample of convective core mass and core hydrogen content inferences (the mass and remaining hydrogen content within the Schwarzschild boundary) for core-hydrogen burning stars from the literature and show them in Fig. 1. The values, their associated uncertainties, and references are listed in Table A.1. The core mass inferences are plotted against predictions from non-rotating models with $Z = 0.014$ and $Y = 0.276$ (computed with MESA r10398; Paxton et al. 2019) with a minimum amount of internal chemical mixing (included in the form of diffusive exponential overshooting with f_{ov}=0.005). The models span $1.1 < M < 25$ $M_\odot$. The colour of the background denotes the remaining fraction of the core-hydrogen content relative to the amount at the zero-age main sequence. The colour of the markers correspond to the inferred fractional core-hydrogen content of that star. If the model predictions were accurate, the colour of the marker would match the colour of the background where the point is situated. Instead, the inferred

values are systematically shifted upwards with respect to their predicted location, indicating that the observations are better reproduced by models with more massive convective cores that are less progressed along their main-sequence evolution. This sample is composed of inferences from p and g mode (and hybrid) pulsating stars, eclipsing binaries, and pulsating stars in binaries, spanning a wide mass range ($1.14 < M < 24$ $M_\odot$).

The diversity of this sample *i*) confirms the robust need for more massive convective cores across a wide stellar mass range, and *ii*) demonstrates that models including only one mixing mechanism with a single efficiency cannot reproduce the range of core masses displayed in Fig. 1. Instead, we find that the range of observations can be reproduced by considering stellar models with internal mixing profiles that span a wide range of efficiencies. This result is consistent with the fact that the observables used in modelling efforts are not directly sensitive to a particular chemical mixing mechanism, but rather to the overall influence of chemical mixing on the stellar temperature, radius, core properties, and near core chemical gradient. Thus, we interpret the diversity of inferred core masses to result from the combined effect of multiple mixing mechanisms active in different stars. We adopt a representative mixing profile consisting of convective boundary mixing in the form of diffusive exponential overshooting (Freytag et al. 1996) with $f_{ov} \in [0.005, 0.04] H_p$, and mixing in the radiative zone induced by internal gravity waves with base efficiencies in the range of $D_{\rm IGW} \in [1 - 100]$ cm^2 s^{-1}. This range is derived by first considering the range of efficiencies for each mechanism reported in the literature, and then trimming the ranges to include all values for which we can reproduce the values reported in Table A.1. We stress that this representative profile and efficiency ranges are only a proxy for the total amount of internal chemical mixing, and should not be considered as absolute metric. We remark instead that this range of efficiencies can be interpreted as arising from different mechanisms producing an overall different effect in different stars.

4. Implications beyond the main sequence

The modification of the convective core mass during the main sequence propagates throughout the remainder of the star's evolution (Stothers & Chin 1981). Kaiser et al. (2020) demonstrated that variable convective boundary mixing efficiencies lead to large differences in the resulting helium-core mass at the terminal-age main sequence (>30%), the carbon/oxygen core mass at the end of core helium burning (up to 70%), and in the observed surface abundances. These differences necessarily have consequences for the stellar end product, although Kaiser et al. (2020) only focused on supernova progenitors. Such variations in stellar end products have also been demonstrated for varying degrees of rapid rotation (Brott et al. 2011a; Ekström et al. 2012), as well as for the inclusion of convective entrainment in 1D models (Scott et al. 2021).

Figure 2 shows the predicted values of the helium core mass at the end of the main sequence for stars between $1.1 \leq M \leq 25$ $M_\odot$. The grey region contains those predicted values for models which include the representative range of chemical mixing efficiencies which reliably reproduces the range of inferred core masses shown in Fig 1. These predictions are compared to predictions by non-rotating MIST (red, Choi et al. 2016) and PARSEC (blue, Bressan et al. 2012) models. The result of this comparison is that we predict a wide range of possible resultant helium core masses, compared to the MIST or PARSEC models which adopt a single efficiency for one chemical mixing mechanism, and that the predicted range of helium core masses increases with mass within the available range.

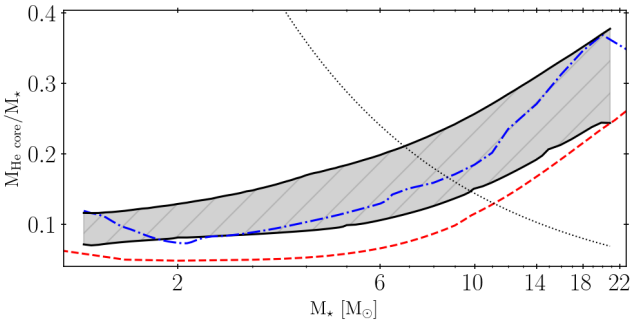


Fig. 2. Predicted helium core mass at the terminal-age main sequence for models with CBM represented by overshooting and internal gravity wave mixing (grey) compared against predictions from MIST models (Choi et al. 2016) in red and PARSEC models (Bressan et al. 2012) in blue. The dotted black line denotes the fractional core mass required to produce a remnant helium core with $M = 1.44$ $M_\odot$.

The prediction of a range of helium core masses has numerous implications beyond main-sequence evolution and to other fields of astronomy. Crucially, this range suggests that there is not a singular one-to-one relation between the birth-mass of the star and the mass of the end-product, as can be seen in the range of the helium core masses. Kaiser et al. (2020) demonstrated that this can have an impact on the results of supernova simulations, but did not consider masses below 15 $M_\odot$. The mass limit for a star to produce a neutron star end-product canonically depends on the remnant core mass exceeding the Chandrasekhar limit of $M_{\rm crit} \approx 1.44$ $M_\odot$. Typically, a remnant core with such a mass is thought to be achieved for stars with initial masses $M_{\rm init} >\sim 8{-}9$ $M_\odot$, considering possible accretion onto the core at later evolutionary stages (Heger et al. 2003; Fryer & Hungerford 2005; Camenzind 2007; Kippenhahn et al. 2012). This limiting mass is denoted by the dotted black line in Fig. 2. Interestingly we see that this critical remnant core mass is already reached for stars with initial masses as low as $M_{\rm init} >\sim 7$ $M_\odot$ for models with the most internal mixing that is considered. This lower limit does not consider possible core mass enhancement through later phases of shell burning or convective boundary mixing during later core burning phases.

Furthermore, studies have demonstrated that convective boundary mixing is favoured to explain observations of evolved single stars (Montalbán et al. 2013; Constantino et al. 2017; Bossini et al. 2017; Arentoft et al. 2017; den Hartogh et al. 2019), and/or binary interaction products, such as subdwarfs (Constantino & Baraffe 2018; Ostrowski et al. 2021). However, the study of binaries and stellar populations is also dependent upon considerations of internal mixing in stellar models. Particularly, the pathways of binary evolution products depend on the radius and central condensation of an evolving star to determine the probability, duration, and efficiency of mass transfer.

5. Conclusions

It is easy to review the results of all the attempts to calibrate different internal mixing mechanisms and think that they disagree. However, given the nature of the sensitivity of modern observables combined with the limitations of 1D stellar models, we argue that these results do agree. Irrespective of the type of internal mixing mechanism implemented, models require a mechanism to modify the core mass, internal chemical gradi-

ents, and surface properties in order to reproduce observations. This is supported by the fact that different studies have been able to independently reproduce the behaviour of commonly used observables with different implementations of mixing mechanisms such as convective penetration, overshooting, entrainment, rotation, and internal gravity waves (Brott et al. 2011b; Ekström et al. 2012; Staritsin 2013; Moravveji et al. 2015; Claret & Torres 2017; Tkachenko et al. 2020; Pedersen et al. 2021; Scott et al. 2021).

Consulting the diversity of results from the literature, it is clear that a wide range of internal mixing efficiencies are required to reproduce observations even when considering a single mixing mechanism. When considering a single efficiency for a single mixing mechanism, models predictions are unintentionally biased. Based on the diverse sample of inferred core masses we have collected, we instead argue that a range of efficiencies needs to be considered to function as a proxy for the various mixing processes present at the convective boundary which are commonly ignored in standard 1D models. As this in turn produces a range of helium core masses at the terminal-age main sequence, this range of efficiencies should be accounted for in evolutionary calculations for both single and binary stars, nucleosynthetic yield predictions, and population synthesis efforts beyond the main sequence.

Acknowledgements. CJ would like to thank the referee for their comments which improved the manuscript. CJ thanks M.G. Pedersen, J.S.G. Mombarg, G. Angelou, L. Viani, and C. Neiner for sharing their results to be included in this manuscript, as well as D.M. Bowman, A. Tkachenko, and C. Aerts for their useful discussion on topics concerning asteroseismology and chemical mixing profiles, and M. Abdul-Masih and A. Escorza for their comments on the manuscript. This work has received funding from NOVA, the European Research Council under the European Union's Horizon 2020 research and innovation programme (N°670519:MAMSIE), and from the Research Foundation Flanders under grant agreement G0A2917N (BlackGEM). The computational resources and services used in this work were provided by the VSC (Flemish Supercomputer Center), funded by the Research Foundation - Flanders (FWO) and the Flemish Government - department EWI to PI Johnston.

References

Aerts, C. 2021, Reviews of Modern Physics, 93, 015001
Aerts, C., Christensen-Dalsgaard, J., & Kurtz, D. W. 2010, Asteroseismology, Astronomy and Astrophysics Library (Springer-Verlag, Heidelberg)
Aerts, C., Molenberghs, G., Michielsen, M., et al. 2018, ApJS, 237, 15
Angelou, G. C., Bellinger, E. P., Hekker, S., et al. 2020, MNRAS, 493, 4987
Arentoft, T., Brogaard, K., Jessen-Hansen, J., et al. 2017, ApJ, 838, 115
Arnett, W. D., Meakin, C., Hirschi, R., et al. 2019, ApJ, 882, 18
Arnett, W. D., Meakin, C., Viallet, M., et al. 2015, ApJ, 809, 30
Bastian, N., Kamann, S., Cabrera-Ziri, I., et al. 2018, MNRAS, 480, 3739
Beasor, E. R., Davies, B., Smith, N., & Bastian, N. 2019, MNRAS, 486, 266
Bertelli, G., Bressan, A. G., & Chiosi, C. 1985, A&A, 150, 33
Böhm-Vitense, E. 1958, ZAp, 46, 108
Bossini, D., Miglio, A., Salaris, M., et al. 2017, MNRAS, 469, 4718
Bouabid, M. P., Dupret, M. A., Salmon, S., et al. 2013, MNRAS, 429, 2500
Bressan, A., Marigo, P., Girardi, L., et al. 2012, MNRAS, 427, 127
Bressan, A. G., Chiosi, C., & Bertelli, G. 1981, A&A, 102, 25
Briquet, M., Aerts, C., Baglin, A., et al. 2011, A&A, 527, A112
Briquet, M., Morel, T., Thoul, A., et al. 2007, MNRAS, 381, 1482
Brott, I., de Mink, S. E., Cantiello, M., et al. 2011a, A&A, 530, A115
Brott, I., Evans, C. J., Hunter, I., et al. 2011b, A&A, 530, A116
Buysschaert, B., Aerts, C., Bowman, D. M., et al. 2018, A&A, 616, A148
Camenzind, M. 2007, Compact objects in astrophysics : white dwarfs, neutron stars, and black holes
Castro, N., Fossati, L., Langer, N., et al. 2014, A&A, 570, L13
Choi, J., Dotter, A., Conroy, C., et al. 2016, ApJ, 823, 102
Claret, A. 2019, A&A, 628, A29
Claret, A. & Giménez, A. 2010, A&A, 519, A57
Claret, A. & Torres, G. 2016, A&A, 592, A15
Claret, A. & Torres, G. 2017, ApJ, 849, 18
Claret, A. & Torres, G. 2018, ApJ, 859, 100
Claret, A. & Torres, G. 2019, ApJ, 876, 134
Constantino, T. & Baraffe, I. 2018, A&A, 618, A177
Constantino, T., Campbell, S. W., & Lattanzio, J. C. 2017, MNRAS, 472, 4900
Costa, G., Girardi, L., Bressan, A., et al. 2019, MNRAS, 485, 4641
Cristini, A., Meakin, C., Hirschi, R., et al. 2017, MNRAS, 471, 279
Deheuvels, S., Bruntt, H., Michel, E., et al. 2010, A&A, 515, A87
Deheuvels, S. & Michel, E. 2011, A&A, 535, A91
den Hartogh, J. W., Eggenberger, P., & Hirschi, R. 2019, A&A, 622, A187
Dupree, A. K., Dotter, A., Johnson, C. I., et al. 2017, ApJ, 846, L1
Ekström, S., Georgy, C., Eggenberger, P., et al. 2012, A&A, 537, A146
Ekström, S., Meynet, G., Georgy, C., & Granada, A. 2018, Memorie della Societa Astronomica Italiana, 89, 50
Freytag, B., Ludwig, H. G., & Steffen, M. 1996, A&A, 313, 497
Fryer, C. L. & Hungerford, A. 2005, in NATO Advanced Study Institute (ASI) Series B, Vol. 210, The Electromagnetic Spectrum of Neutron Stars, 3
Georgy, C., Charbonnel, C., Amard, L., et al. 2019, A&A, 622, A66
Gosnell, N. M., Mathieu, R. D., Geller, A. M., et al. 2015, ApJ, 814, 163
Guinan, E. F., Ribas, I., Fitzpatrick, E. L., et al. 2000, ApJ, 544, 409
Handler, G. 2013, Asteroseismology, ed. T. D. Oswalt & M. A. Barstow, Vol. 4, 207
Heger, A., Fryer, C. L., Woosley, S. E., Langer, N., & Hartmann, D. H. 2003, ApJ, 591, 288
Higl, J., Müller, E., & Weiss, A. 2021, A&A, 646, A133
Higl, J. & Weiss, A. 2017, A&A, 608, A62
Hirschi, R., den Hartogh, J., Cristini, A., Georgy, C., & Pignatari, M. 2014, in XIII Nuclei in the Cosmos (NIC XIII), 1
Johnston, C., Aerts, C., Pedersen, M. G., & Bastian, N. 2019a, A&A, 632, A74
Johnston, C., Aimar, N., Abdul-Masih, M., et al. 2021, MNRAS, 503, 1124
Johnston, C., Pavlovski, K., & Tkachenko, A. 2019b, A&A, 628, A25
Johnston, C., Tkachenko, A., Aerts, C., et al. 2019c, MNRAS, 482, 1231
Kaiser, E. A., Hirschi, R., Arnett, W. D., et al. 2020, MNRAS, 496, 1967
Kamann, S., Bastian, N., Husser, T. O., et al. 2018, MNRAS, 480, 1689
Kippenhahn, R., Weigert, A., & Weiss, A. 2012, Stellar Structure and Evolution (Springer-Verlag Berlin Heidelberg)
Langer, N. 2012, ARA&A, 50, 107
Maeder, A. 2009, Physics, Formation and Evolution of Rotating Stars (Springer-Verlag Berlin Heidelberg)
Maeder, A. & Meynet, G. 1987, A&A, 182, 243
Martinet, S., Meynet, G., Ekström, S., et al. 2021, A&A, 648, A126
Mazumdar, A., Briquet, M., Desmet, M., & Aerts, C. 2006, A&A, 459, 589
Meakin, C. A. & Arnett, D. 2007, ApJ, 667, 448
Michielsen, M., Pedersen, M. G., Augustson, K. C., Mathis, S., & Aerts, C. 2019, A&A, 628, A76
Miglio, A., Montalbán, J., Noels, A., & Eggenberger, P. 2008, MNRAS, 386, 1487
Mombarg, J. S. G., Van Reeth, T., & Aerts, C. 2021, A&A, 650, A58
Mombarg, J. S. G., Van Reeth, T., Pedersen, M. G., et al. 2019, MNRAS, 485, 3248
Montalbán, J., Miglio, A., Noels, A., et al. 2013, ApJ, 766, 118
Moravveji, E., Aerts, C., Pápics, P. I., Triana, S. A., & Vandoren, B. 2015, A&A, 580, A27
Moravveji, E., Townsend, R. H. D., Aerts, C., & Mathis, S. 2016, ApJ, 823, 130
Noll, A., Deheuvels, S., & Ballot, J. 2021, A&A, 647, A187
Ostrowski, J., Baran, A. S., Sanjayan, S., & Sahoo, S. K. 2021, MNRAS, 503, 4646
Paxton, B., Smolec, R., Schwab, J., et al. 2019, ApJS, 243, 10
Pedersen, M. G., Aerts, C., Pápics, P. I., et al. 2021, Nature Astronomy [arXiv:2105.04533]
Pedersen, M. G., Aerts, C., Pápics, P. I., & Rogers, T. M. 2018, A&A, 614, A128
Pols, O. R., Tout, C. A., Schroder, K.-P., & Eggleton. 1997, MNRAS, 289, 869
Renzini, A. 1987, A&A, 188, 49
Ribas, I., Jordi, C., & Giménez, Á. 2000, MNRAS, 318, L55
Rogers, T. M. & McElwaine, J. N. 2017, ApJ, 848, L1
Salaris, M. & Cassisi, S. 2017, Royal Society Open Science, 4, 170192
Salmon, S., Montalbán, J., Morel, T., et al. 2012, MNRAS, 422, 3460
Schmid, V. S. & Aerts, C. 2016, A&A, 592, A116
Schneider, F. R. N., Izzard, R. G., de Mink, S. E., et al. 2014a, ApJ, 780, 117
Schneider, F. R. N., Langer, N., de Koter, A., et al. 2014b, A&A, 570, A66
Schroder, K.-P., Pols, O. R., & Eggleton, P. P. 1997, MNRAS, 285, 696
Scott, L. J. A., Hirschi, R., Georgy, C., et al. 2021, MNRAS, 503, 4208
Sekaran, S., Tkachenko, A., Johnston, C., & Aerts, C. 2021, A&A, 648, A91
Serenelli, A., Weiss, A., Aerts, C., et al. 2021, A&A Rev., 29, 4
Silva Aguirre, V., Ballot, J., Serenelli, A. M., & Weiss, A. 2011, A&A, 529, A63
Stancliffe, R. J., Fossati, L., Passy, J. C., & Schneider, F. R. N. 2015, A&A, 575, A117
Staritsin, E. I. 2013, Astronomy Reports, 57, 380
Stothers, R. & Chin, C. W. 1981, ApJ, 247, 1063
Szewczuk, W. & Daszyńska-Daszkiewicz, J. 2018, MNRAS, 478, 2243
Tkachenko, A., Pavlovski, K., Johnston, C., et al. 2020, A&A, 637, A60
Torres, G., Andersen, J., & Giménez, A. 2010, ARA&A, 18, 67
Valle, G., Dell'Omodarme, M., Prada Moroni, P. G., & Degl'Innocenti, S. 2017, A&A, 600, A41
Valle, G., Dell'Omodarme, M., Prada Moroni, P. G., & Degl'Innocenti, S. 2018, A&A, 615, A62
VandenBerg, D. A., Bergbusch, P. A., & Dowler, P. D. 2006, ApJS, 162, 375
Viani, L. S. & Basu, S. 2020, ApJ, 904, 22
Yang, W. & Tian, Z. 2017, ApJ, 836, 102

Appendix A: Sample

Table A.1. Sample of estimated stellar masses and inferred convective core masses and fractional core-hydrogen content.

Star	Mass [$M_\odot$]	M_{cc} [$M_\odot$]	X_c/X_{ini}		Star	Mass [$M_\odot$]	M_{cc} [$M_\odot$]	X_c/X_{ini}	
KIC 12009504	1.19 ± 0.07	0.08 ± 0.02	0.21	(a)	KIC 7760680	$3.37^{+0.01}_{-0.06}$	$0.62^{+0.02}_{-0.00}$	0.53	(c)
KIC 6225718	1.26 ± 0.03	0.08 ± 0.04	0.60	(a)	KIC 8057661	$9.52^{+0.02}_{-0.03}$	$1.76^{+0.01}_{-0.01}$	0.18	(c)
KIC 10454113	1.27 ± 0.02	0.08 ± 0.03	0.59	(a)	KIC 8255796	$5.73^{+0.10}_{-0.03}$	$0.49^{+0.10}_{-0.00}$	0.02	(c)
KIC 5184732	1.20 ± 0.01	0.06 ± 0.001	0.26	(a)	KIC 8381949	$6.27^{+0.79}_{-0.00}$	$1.53^{+0.07}_{-0.10}$	0.57	(c)
KIC 12009504	1.20 ± 0.01	0.07 ± 0.02	0.21	(a)	KIC 8459899	$3.36^{+0.00}_{-0.03}$	$0.84^{+0.03}_{-0.00}$	0.34	(c)
KIC 7206837	1.44 ± 0.04	0.17 ± 0.03	0.41	(a)	KIC 8714886	$6.49^{+0.00}_{-0.08}$	$0.92^{+0.01}_{-0.00}$	0.28	(c)
KIC 12258514	1.24 ± 0.02	0.09 ± 0.01	0.07	(a)	KIC 8766405	$3.49^{+0.00}_{-0.23}$	$0.55^{+0.03}_{-0.00}$	0.22	(c)
KIC 7510397	1.36 ± 0.04	0.11 ± 0.03	0.09	(a)	KIC 9020774	$3.41^{+0.21}_{-0.28}$	$0.70^{+0.07}_{-0.17}$	0.78	(c)
KIC 8228742	1.33 ± 0.05	0.11 ± 0.01	0.06	(a)	KIC 9715425	$4.72^{+0.45}_{-0.20}$	$0.91^{+0.01}_{-0.06}$	0.48	(c)
KIC 2710594	$1.50^{+0.13}_{-0.09}$	$0.16^{+0.01}_{-0.01}$	0.67	(b)	KIC 10526294	$3.64^{+0.10}_{-0.21}$	$0.41^{+0.01}_{-0.06}$	0.23	(c)
KIC 3448365	$1.49^{+0.01}_{-0.07}$	$0.12^{+0.01}_{-0.01}$	0.63	(b)	KIC 10536147	$7.50^{+0.07}_{-0.41}$	$2.17^{+0.06}_{-0.14}$	0.98	(c)
KIC 4846809	$1.49^{+0.05}_{-0.02}$	$0.15^{+0.01}_{-0.01}$	0.58	(b)	KIC 11360704	$4.47^{+1.54}_{-0.00}$	$1.20^{+0.00}_{-0.66}$	0.47	(c)
KIC 5114382	$1.61^{+0.02}_{-0.14}$	$0.16^{+0.01}_{-0.01}$	0.36	(b)	KIC 11971405	$3.67^{+0.21}_{-0.72}$	$0.62^{+0.11}_{-0.03}$	0.46	(c)
KIC 5522154	$1.72^{+0.28}_{-0.22}$	$0.19^{+0.03}_{-0.02}$	0.97	(b)	KIC 12258330	$3.53^{+0.04}_{-0.13}$	$0.69^{+0.03}_{-0.00}$	0.68	(c)
KIC 5708550	$1.99^{+0.01}_{-0.61}$	$0.20^{+0.01}_{-0.06}$	0.98	(b)	KIC 4930889 A	$4.89^{+1.49}_{-1.09}$	0.54	0.07	(d)
KIC 5788623	$1.47^{+0.01}_{-0.05}$	$0.12^{+0.01}_{-0.01}$	0.70	(b)	KIC 4930889 B	$3.47^{+1.40}_{-0.57}$	0.60	0.68	(d)
KIC 6468146	$1.59^{+0.01}_{-0.04}$	$0.17^{+0.01}_{-0.01}$	0.61	(b)	KIC 6352430 A	$3.23^{+1.98}_{-0.56}$	0.56	0.59	(d)
KIC 6468987	$1.57^{+0.13}_{-0.16}$	$0.20^{+0.02}_{-0.02}$	0.74	(b)	KIC 6352430 B	$1.34^{+0.68}_{-1.14}$	0.08	0.77	(d)
KIC 6678174	$1.77^{+0.23}_{-0.22}$	$0.18^{+0.02}_{-0.02}$	0.20	(b)	KIC 10080943 A	$1.99^{+0.37}_{-0.49}$	0.15	0.08	(d)
KIC 6935014	$1.45^{+0.03}_{-0.03}$	$0.16^{+0.01}_{-0.01}$	0.86	(b)	KIC 10080943 B	$1.85^{+0.41}_{-0.45}$	0.17	0.30	(d)
KIC 6953103	$1.88^{+0.12}_{-0.19}$	$0.25^{+0.02}_{-0.03}$	0.48	(b)	V578 Mon A	14.55 ± 0.09	5.12 ± 0.44	0.82	(e)
KIC 7023122	$1.51^{+0.00}_{-0.04}$	$0.16^{+0.01}_{-0.01}$	0.96	(b)	V578 Mon B	10.30 ± 0.06	3.21 ± 0.37	0.89	(e)
KIC 7365537	$1.70^{+0.30}_{-0.26}$	$0.18^{+0.03}_{-0.03}$	0.97	(b)	V453 Cyg A	14.95 ± 0.35	4.81 ± 0.35	0.41	(e)
KIC 7380501	$1.72^{+0.00}_{-0.35}$	$0.14^{+0.01}_{-0.03}$	0.19	(b)	V453 Cyg B	11.91 ± 0.57	3.66 ± 0.53	0.66	(e)
KIC 7434470	$1.48^{+0.01}_{-0.16}$	$0.17^{+0.01}_{-0.02}$	0.64	(b)	V478 Cyg A	16.74 ± 0.73	6.04 ± 0.85	0.58	(e)
KIC 7583663	$1.47^{+0.27}_{-0.16}$	$0.16^{+0.03}_{-0.02}$	0.64	(b)	V478 Cyg B	16.39 ± 0.71	5.97 ± 0.84	0.57	(e)
KIC 7939065	$1.48^{+0.02}_{-0.06}$	$0.14^{+0.00}_{-0.01}$	0.66	(b)	AH Cep A	16.26 ± 0.18	6.20 ± 0.62	0.74	(e)
KIC 8364249	$1.52^{+0.23}_{-0.05}$	$0.17^{+0.03}_{-0.01}$	0.66	(b)	AH Cep B	14.86 ± 0.70	5.22 ± 0.77	0.70	(e)
KIC 8375138	$1.47^{+0.05}_{-0.07}$	$0.15^{+0.01}_{-0.01}$	0.69	(b)	V346 Cen A	13.76 ± 0.40	4.14 ± 0.35	0.36	(e)
KIC 8645874	$1.52^{+0.02}_{-0.01}$	$0.14^{+0.01}_{-0.01}$	0.88	(b)	V346 Cen B	8.40 ± 0.10	2.04 ± 0.35	0.73	(e)
KIC 8836473	$1.48^{+0.11}_{-0.01}$	$0.14^{+0.01}_{-0.01}$	0.34	(b)	V573 Car A	16.62 ± 0.45	6.65 ± 0.45	0.87	(e)
KIC 9480469	$1.49^{+0.05}_{-0.11}$	$0.14^{+0.01}_{-0.01}$	0.82	(b)	V573 Car B	12.49 ± 0.17	4.37 ± 0.32	0.95	(e)
KIC 9595743	$1.42^{+0.03}_{-0.04}$	$0.09^{+0.01}_{-0.01}$	0.94	(b)	V1032 Sco A	18.97 ± 0.77	7.44 ± 0.89	0.60	(e)
KIC 9751996	$1.74^{+0.01}_{-0.02}$	$0.17^{+0.01}_{-0.01}$	0.29	(b)	V1032 Sco B	10.47 ± 0.24	3.29 ± 0.24	0.87	(e)
KIC 10467146	$1.77^{+0.02}_{-0.27}$	$0.16^{+0.01}_{-0.02}$	0.22	(b)	V380 Cyg A	15.00 ± 0.50	3.85 ± 0.15	0.00	(e)
KIC 11080103	$1.53^{+0.02}_{-0.09}$	$0.16^{+0.01}_{-0.01}$	0.76	(b)	V380 Cyg B	8.32 ± 0.75	2.26 ± 0.59	0.78	(e)
KIC 11099031	$1.57^{+0.03}_{-0.21}$	$0.17^{+0.01}_{-0.02}$	0.41	(b)	CW Cep A	13.01 ± 0.07	4.38 ± 0.62	0.77	(e)
KIC 11294808	$1.45^{+0.20}_{-0.04}$	$0.13^{+0.02}_{-0.00}$	0.27	(b)	CW Cep B	11.95 ± 0.09	3.86 ± 0.48	0.79	(e)
KIC 11456474	$1.49^{+0.14}_{-0.13}$	$0.13^{+0.01}_{-0.01}$	0.25	(b)	U Oph A	5.10 ± 0.05	1.01 ± 0.11	0.65	(e)
KIC 11721304	$1.43^{+0.04}_{-0.03}$	$0.15^{+0.01}_{-0.01}$	0.89	(b)	U Oph B	4.60 ± 0.05	0.93 ± 0.08	0.74	(e)
KIC 11754232	$1.53^{+0.02}_{-0.04}$	$0.15^{+0.01}_{-0.01}$	0.90	(b)	V621 Per A	11.81 ± 0.30	2.80 ± 0.21	0.84	(e)
KIC 11907454	$1.47^{+0.01}_{-0.10}$	$0.13^{+0.01}_{-0.01}$	0.83	(b)	HD165246 B	$3.8^{+0.4}_{-0.5}$	$0.42^{+0.4}_{-0.2}$	1.00	(f)
KIC 11826272	$1.52^{+0.04}_{-0.07}$	$0.16^{+0.01}_{-0.01}$	0.51	(b)	HD165246 A	$23.7^{+1.1}_{-1.4}$	$10.2^{+1.3}_{-1.6}$	0.76	(f)
KIC 11917550	$1.51^{+0.00}_{-0.10}$	$0.16^{+0.01}_{-0.01}$	0.67	(b)	2052 Oph	8.9 ± 0.7	1.70 ± 0.2	0.41	(g)
KIC 11920505	$1.45^{+0.03}_{-0.01}$	$0.11^{+0.01}_{-0.01}$	0.88	(b)	HD 43317	$5.8^{+0.1}_{-0.2}$	1.33 ± 0.05	0.76	(h)
KIC 12066947	$1.49^{+0.02}_{-0.01}$	$0.14^{+0.01}_{-0.01}$	0.65	(b)	HIC 12258514	1.20 ± 0.05	0.05 ± 0.01		(i)
KIC 3240411	$5.34^{+0.31}_{-0.07}$	$1.56^{+0.00}_{-0.02}$	0.68	(c)	KIC 8228742	1.25 ± 0.08	0.06 ± 0.02		(i)
KIC 3459297	$3.70^{+0.00}_{-0.18}$	$0.24^{+0.01}_{-0.01}$	0.05	(c)	KIC 7510397	1.22 ± 0.06	0.07 ± 0.03		(i)
KIC 3865742	$5.66^{+0.00}_{-0.08}$	$1.05^{+0.03}_{-0.00}$	0.22	(c)	KIC 10162436	1.30 ± 0.06	0.09 ± 0.02		(i)
KIC 4936089	$3.66^{+0.01}_{-0.00}$	$0.43^{+0.00}_{-0.00}$	0.35	(c)	KIC 5773345	1.49 ± 0.09	0.15 ± 0.01		(i)
KIC 4939281	$5.38^{+1.18}_{-0.34}$	$1.31^{+0.01}_{-0.27}$	0.48	(c)	KIC 3456181	1.39 ± 0.07	0.11 ± 0.03		(i)
KIC 5309849	$5.67^{+0.01}_{-0.00}$	$0.75^{+0.00}_{-0.00}$	0.15	(c)	KIC 8179536	1.22 ± 0.09	0.03 ± 0.03		(i)
KIC 5941844	$3.75^{+0.03}_{-0.02}$	$0.90^{+0.04}_{-0.27}$	0.94	(c)	β Cma	13.5 ± 0.5	3.5 ± 0.3	0.18	(j)
KIC 6462033	$7.45^{+0.13}_{-0.00}$	$1.08^{+0.05}_{-0.00}$	0.17	(c)	β Cru	14.5 ± 0.5	4.13 ± 0.5	0.27	(k)
KIC 6780397	$6.29^{+0.01}_{-0.00}$	$0.55^{+0.00}_{-0.00}$	0.05	(c)	KIC 9850387	1.66 ± 0.01	0.16 ± 0.01	0.24	(l)
KIC 7630417	$6.92^{+0.01}_{-0.00}$	$0.91^{+0.00}_{-0.00}$	0.15	(c)					

References. (a) Angelou et al. 2020 ; (b) Mombarg et al. 2021 ; (c) Pedersen et al. 2021 ; (d) Johnston et al. 2019c; (e) Tkachenko et al. 2020; (f) Johnston et al. 2021; (g) Briquet et al. 2011; (h) Buysschaert et al. 2018; (i) Viani & Basu 2020; (j) Mazumdar et al. 2006; (k) Cotton et al. *in review*; (l) Sekaran et al. 2021